

Article

Inconsistency Detection in Cross-Layer Tile Maps with Super-Pixel Segmentation

Junbo Yu ¹ , Tinghua Ai ^{1,2,3,*} , Haijiang Xu ¹, Lingrui Yan ¹ and Yilang Shen ⁴

¹ School of Resource and Environmental Sciences, Wuhan University, Wuhan 430079, China

² Key Laboratory of Geographic Information System, Ministry of Education, Wuhan 430079, China

³ Key Laboratory of Digital Mapping and Land Information Application Engineering, National Administration of Surveying, Mapping and Geo-Information, Wuhan 430079, China

⁴ School of Geospatial Engineering and Science, Sun Yat-sen University, Zhuhai 519082, China

* Correspondence: tinghuaai@whu.edu.cn; Tel.: +86-139-0863-9199

Abstract: The consistency of geospatial data is of great significance for the application and updating of geographic information in web maps. Due to the multiple data sources and different temporal versions, the tile web maps usually meet the inconsistency question across different layers. This study tries to develop a method to detect this kind of inconsistency utilizing a raster-based scaling approach. Compared with vector-based handling, this method can be directly available for multi-level tile images in a pixel representation form. The proposed cross-layer raster tile map rendering method (CRTMRM) consists of four primary aspects: geographic object separation, consistency rendering rules, data scaling and derivation with super-pixel segmentation, and inconsistency detection. The scale transformation strategy with the super-pixel attempts to obtain a simplified representation. Taking the scale lifespan variation and geometric consistency rules into account, the inconsistency detection of tile maps is conducted between temporal versions, multi-sources, and different scales through actual and derived data overlay analysis. The experiment focuses on features of cross-layer water or vegetation areas with Level 9 to Level 14 in Baidu Maps, Amap, and Google Maps. This method is able to serve as a basis for massive unstructured web map data inconsistency detection and support intelligent web map rendering.

Keywords: consistency detection; tile map; super-pixel; map generalization; web map rendering



Citation: Yu, J.; Ai, T.; Xu, H.; Yan, L.; Shen, Y. Inconsistency Detection in Cross-Layer Tile Maps with Super-Pixel Segmentation. *ISPRS Int. J. Geo-Inf.* **2023**, *12*, 244. <https://doi.org/10.3390/ijgi12060244>

Academic Editors: Florian Hruby and Wolfgang Kainz

Received: 20 March 2023

Revised: 6 June 2023

Accepted: 15 June 2023

Published: 17 June 2023



Copyright: © 2023 by the authors. Licensee MDPI, Basel, Switzerland. This article is an open access article distributed under the terms and conditions of the Creative Commons Attribution (CC BY) license (<https://creativecommons.org/licenses/by/4.0/>).

1. Introduction

The pre-rendering mechanism and the pioneering idea for map tile segmentation have comprehensively boosted the web map experience, especially with the release of Google Maps API. Whether it is the integration of real-time road conditions [1], street view data [2], 3D models [3], or mobile cartography [4], each period of web map rendering technology has invariably facilitated the ubiquity of web maps [5–7]. Meanwhile, the tile pyramid technique has been increasingly adopted for various web maps for its advantages of storage and fast transmission speed [8–10]. The tile map is effectively represented by several small images of the same size (usually 256 × 256 pixels) seamlessly stitched following defined rules [11]. When panning or zooming, it is accessed and displayed on the web per the pyramid rules, and it can usually be categorized into raster and vector tiles [12]. Currently, tile maps have been broadly applied in numerous fields, such as geographic boundaries [13], landscape ecology [14], topography [15], and land cover products [16]. The Internet map and tile pyramid organization have significantly contributed to the map application. However, a crucial concern of tile maps is geospatial data quality.

Accompanied by the massive web service media, and data integration or updates in different representations, the multi-temporal, multi-source, and multi-scale characteristics of geographic data from multi-level tile maps may lead to spatial data quality problems [17], such as the inconsistency between tile layers. Several major reasons for this condition are

as follows: (1) the contradiction between the instantaneous landscape changes and the lagging data collection or processing period; (2) diverse geographic information standards or map production periods from different authorities; and (3) complicated patterns of intricate dimensional or morphological changes from the geospatial data when displayed in cross-layer tile maps. Significantly, the inconsistent visualization of tile maps may not only puzzle users for geospatial elements perception but also cause map matching conflicts or map design obstacles for cartographers during the data processing from multi-source web data. In the case of water rendering from cross-layer tile maps, as shown in Figure 1, narrow rivers are prone to discontinuity or curved rivers intertwining and overlapping in low-level map representation. The first and foremost step to avoid such problems is to conduct cross-layer tile map inconsistency detection.

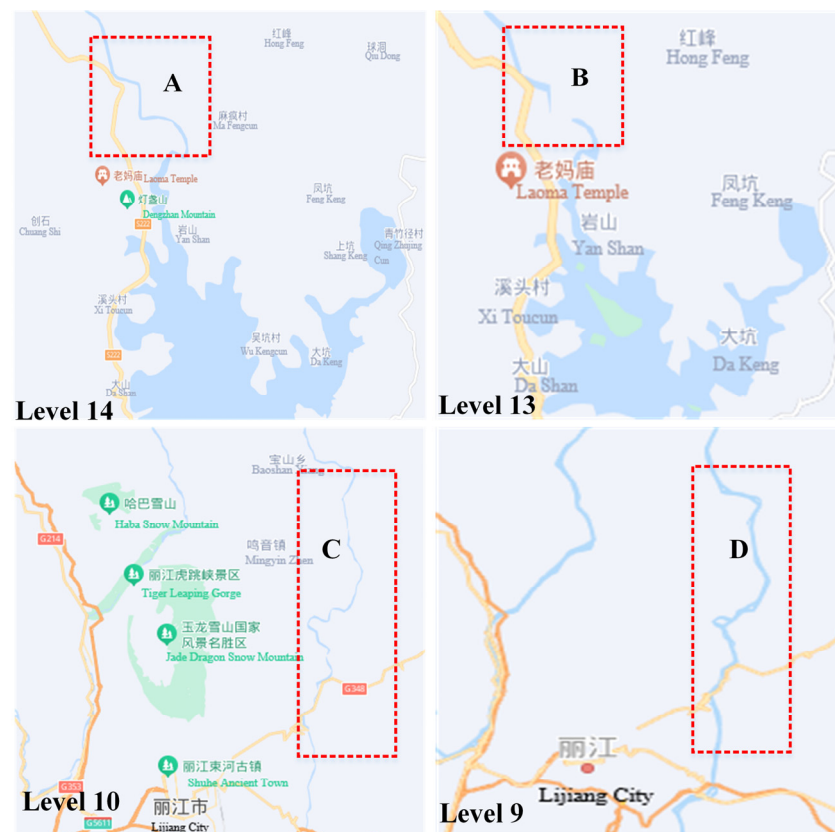


Figure 1. Inconsistencies during the tile map rendering at different levels. (A,B): river breakage in low-level representation; (C,D): overlapping rivers.

In response to the demand for cross-layer map consistency visualization, vector structure-based techniques are commonly available. However, the raster-structured tile image is usually available for end-display and accessibility directly by web maps. When judging inconsistency, the initiative of converting them to a vector before utilizing point, line, and polygon structure approaches is bound to be a cumbersome process. The most desirable way to detect the inconsistency from cross-layer tile maps is to perform it directly in a raster pattern.

The previous vector methods have been broadly applied for various types of inconsistency detection, such as geometric forms, spatial relationships, and semantic features. First, the geometric inconsistency is mainly manifested in its location and shape. The former mainly combines coordinate conversion, map projection, and alignment methods when the inconsistency detection is for same-scale geospatial data [18–21]. Meanwhile, the latter inconsistency detection for cross-scale geographic objects is fulfilled through spatial or knowledge databases [22,23]. Moreover, it is also quite typical to quantify and detect

inconsistencies or changes in geospatial data through object matching [24] or map algebra [25]. Second, the spatial relationship inconsistency is mostly reflected in the topological or logical conflict of geographical objects. This type of inconsistency can be detected by spatial object reasoning [26], the nine-intersection model [27], the dimension graph [28], visualization [29], complex regions with broad boundaries [30], and directional relations [31]. Third, the semantic inconsistency is usually caused by cognitive differences [32]. It has been currently well detected and dealt with through measuring semantic similarity [33], matching two-dimensional entities from geographic databases [34], and graph modeling [35]. Furthermore, many scholars have also carried out corresponding data consistency studies on common geospatial data such as roads [36], rivers and contours [37,38], and location maps [39]. The above information reveals the fact that a majority of inconsistency detection is directly based on vector methods, while raster-based methods are rare.

By contrast to vector-pattern data inconsistency detection, raster-pattern inconsistency detection is direct and widely applied in the image process [40] and remote sensing [41]. Moreover, the popular spotlight on past raster methods for detecting data inconsistencies has been on discrepancies due to data sources or time differences, either constructing spatial relationships through feature descriptor similarity based on traditional point-line-polygon attributes [42–45] or changing information updating from historical and current multi-source vector data [46–48], all of which have guided the inconsistency detection of geospatial data in image patterns. In addition, the novel feature matching based on deep learning nowadays enables more flexible geographic data consistency processing [49]. Fortunately, the scale transformation in map rendering is similar to the interconversion between high-resolution and low-resolution remote sensing data [50–52]. In this context, the role of scale transformation in cross-layer tile map rendering and inconsistency detection needs to be strengthened. Undoubtedly, raster-based approaches have recently demonstrated substantial potential for cross-layer map change information processing as well, for example, by taking into account the integrated cartographic generalization scenario of water for consistency detection [53]. In addition, the super-pixel has gradually emerged into researchers' horizons as a novel raster-based method to handle map data across scales [54]. Similar to the vector-based map scale transformation, super-pixel segmentation and merging is also a process of feature simplification representation. The major attraction is that super-pixel segmentation can directly operate on discretized pixels. Therefore, it deserves further expanding how super-pixel segmentation may be applied to acquire cross-layer map tiles that conform to the scale transformation rules in tile map inconsistency detection.

The aforementioned studies have been devoted to tackling the related challenges, and most of those have been devoted to detecting data inconsistency from an object vector-model perspective or changing information from a raster pixel. Nevertheless, the distribution characteristics and geometric features of geographic objects in cross-layer tiles are also worth exploring. The following critical issues still need to be considered in consistency detection across layer tiles:

- (1) The application purpose between the image process and structured map data.
- (2) The balance between reasonable change from scale transformation and inconsistent change by the mistake process.
- (3) The difference between vector-based and raster-based processing patterns to detect inconsistency.

Hence, it is urgent to explore an approach to detect cross-layer geospatial data quality issues directly on the raster pixels of tile maps. In this context, the primary goal of this study is to develop a cross-layer raster tile map rendering method (CRTMRM) that supports raster-based structure scaling to detect the cross-layer geospatial data inconsistency during web map rendering. To realize this purpose, a detection and scaling method based on super-pixel segmentation is applied to derive the rendering data to facilitate the cross-layer tile map inconsistency detection. The framework involves four essential procedures: geographic object separation from tile maps; consistency rendering rules construction

of cross-layer tile maps; data scaling and derivation with super-pixel segmentation; and inconsistency detection for cross-layer tile maps.

The rest of this paper is organized as follows: the study area, test data, and a cross-layer raster tile map rendering method (CRTMRM) are introduced in Section 2, after which the implementation procedure is described in detail. In Section 3, the experimental results are presented in sequence. Some feasibility and directions for inconsistency detection from cross-layer tile maps are discussed in Section 4, while conclusions are shown in Section 5.

2. Materials and Methods

Multi-level tile map rendering involves some coherent processes, such as data model construction, scale transformation, and graphic design of geographic objects. The data quality of cross-layer tile maps is often affected by parameters such as the variation of tile maps, rules, or quality of cartographic generalization. In this study, a cross-layer raster tile map rendering method (CRTMRM) is proposed, as shown in Figure 2. It consists of four procedures: (a) geographic object recognition from tile maps; (b) consistency rendering rules construction of cross-layer tile maps; (c) data scaling and derivation with super-pixel segmentation; (d) inconsistency detection for cross-layer tile maps.

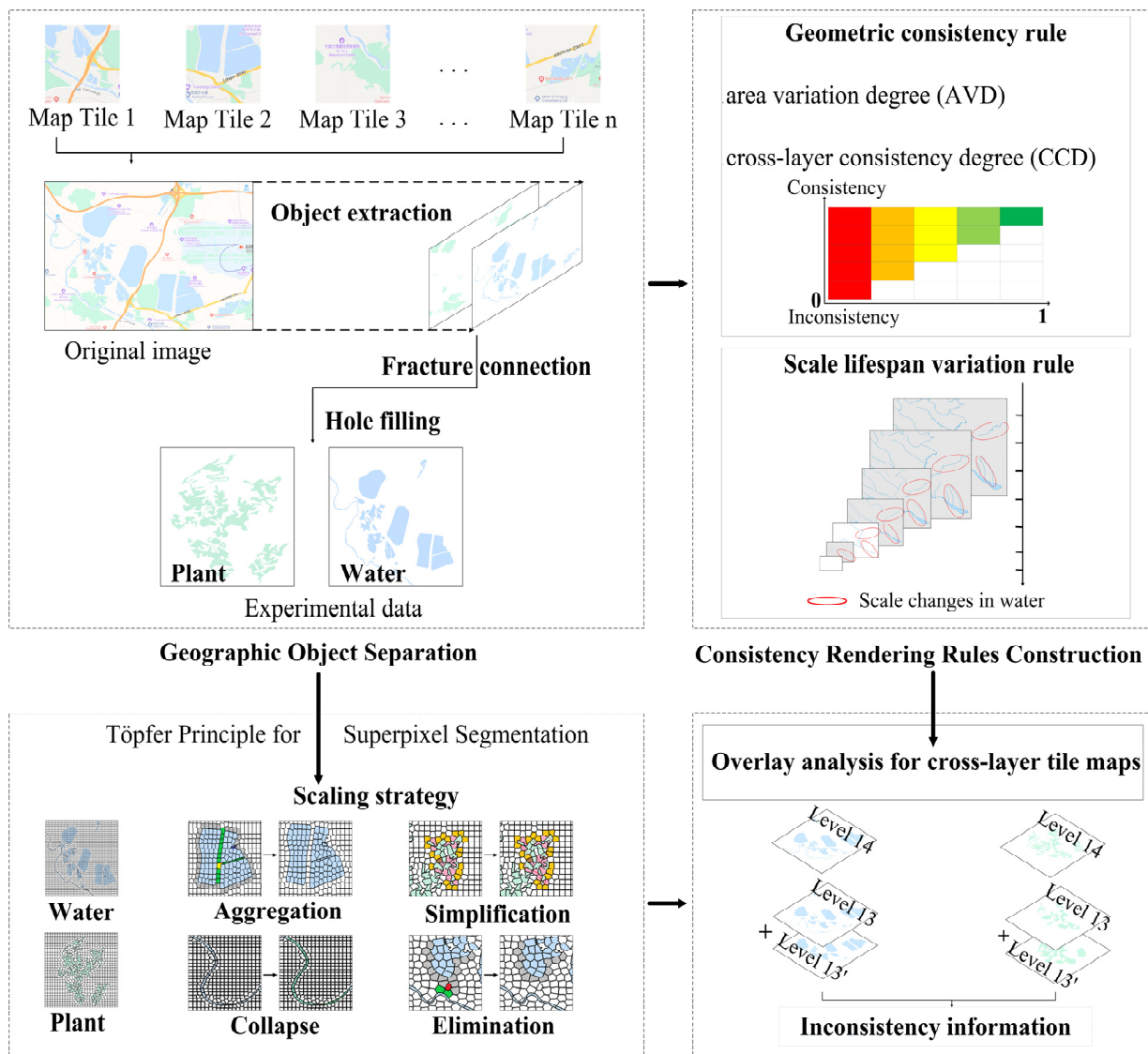


Figure 2. A cross-layer raster tile map rendering method (CRTMRM) for data inconsistency detection.

2.1. Study Area and Data

The raw water and vegetation data from the Baidu map of China are used in this study. These cross-layer tile maps can be downloaded for free through the corresponding uniform resource locator (URL). For instance, the tile data of Level 14 in Baidu Maps whose location is at ($x = 3096$, $y = 620$) can be downloaded via the following URL: https://maponline0.bdimg.com/tile/?qt=vtile&x=3096&y=620&z=14&styles=pl&scaler=1&udt=20221129&from=jsapi2_0, accessed on 29 November 2022. The original data of water and vegetation areas applied in this study are both located at Level 14, and the data that require inconsistency detection are both located at Level 13. The water areas displayed in Figure 3a,b are located near Windsor Great Park in London, U.K. Meanwhile, the vegetation comes from the area near Shinshoji Temple in Naritasan, Japan, as illustrated in Figure 3c,d.

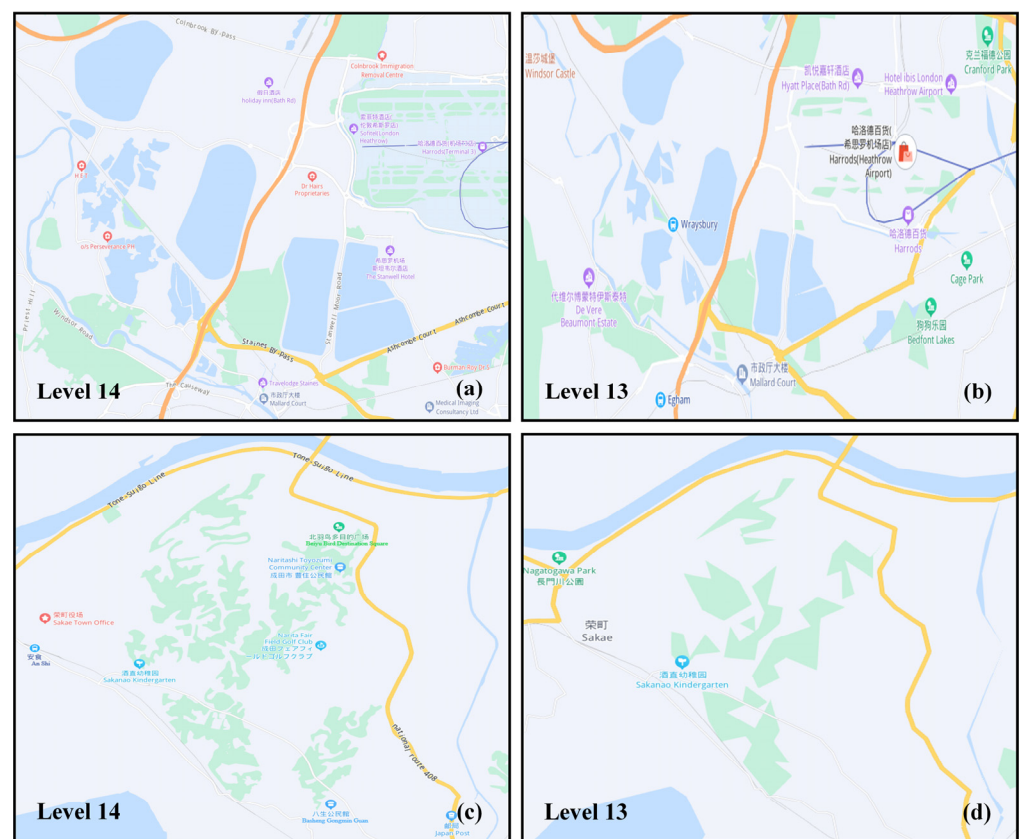


Figure 3. Study area: (a,b) show the water area at Level 14 and Level 13 from the Baidu map, respectively; (c,d) represent the vegetation area at Level 14 and Level 13 from the Baidu map, respectively.

2.2. Geographic Object Separation from Tile Maps

Geographic object recognition has been concerned with extracting isolated areas such as water and vegetation from tile maps. However, there are difficulties in directly separating complete geographic objects from tile maps. It is due to the circumstance that geographic objects are covered by some map notations or are overlaying each other during the zooming process. As a result, the extracted geographical objects may be partly fractured or have holes in them. Fortunately, for a given tile map, the different geographical objects are usually rendered with a uniform color. Therefore, color segmentation is the first step to identifying geographic objects. After getting an initial separation of areas, we need to complete the joining of fractured areas and the filling of holes. After obtaining the initial separated areas, the connection of fractured areas and hole filling are required to be completed.

2.2.1. Fractured Area Connection

The waters themselves are connected, but the direct extraction of rivers or lakes is prone to disconnection due to symbolic overlays such as roads. The closing operation in morphology may enable the connection of partially fractured areas to obtain a more integrated and continuous water area. Assume that an original tile map is A with fractured regions and S is a structural element in Equation (1). Then, the fractured targets will be merged and connected by a dilating and eroding operation in sequence. Its specific process is depicted in Figure 4.

$$A \cdot S = (A \oplus S) \ominus S \tag{1}$$

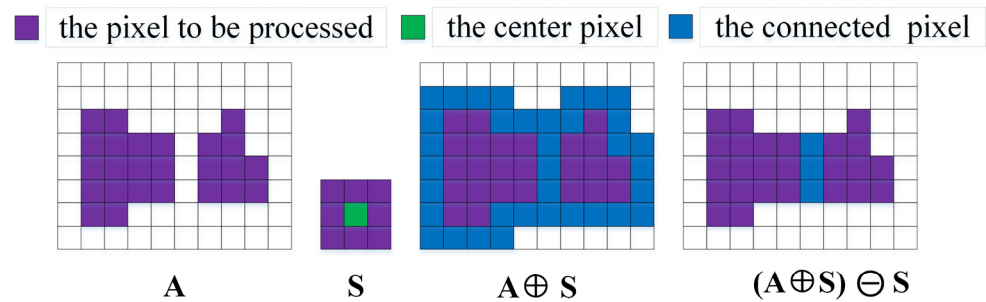


Figure 4. The fracture region connection with the closing operation.

2.2.2. Hole Filling

The direct extraction of enclosed waters or vegetation may result in holes owing to the overlay of place name notations on the web map. The approach of morphological operations is also implemented to fill the hole region of the extracted geospatial data. As displayed in Figure 5, the original map X with the hole is assumed. Its complement set is Y and S is a structural element. The filling process starts with a matrix M₀, whose size is the same as the size of the area containing X, after which the process of Equation (2) is performed to fill the holes. When M_i = M_{i-1}, then the hole filling ends at step i of the iteration. The union of M_i and X is UX = M_i ∪ X, it is the result after the hole filling of the tile map.

$$M_i = (M_{i-1} \oplus S) \cap Y \quad i = 1, 2, 3 \dots \tag{2}$$

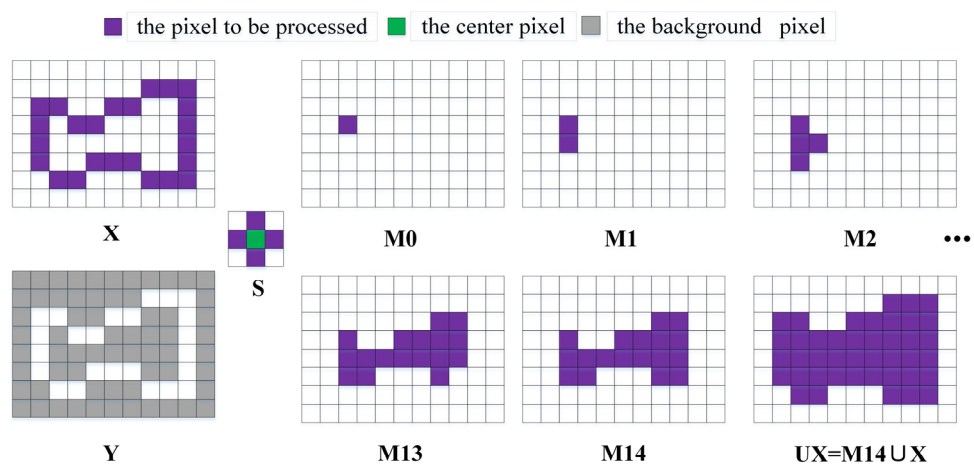


Figure 5. The hole area filling of geospatial data.

2.3. Consistency Rendering Rules for Cross-Layer Tile Maps

Aiming at the characteristics of geospatial data representation in multi-level tile maps, it is necessary to establish consistency rules for geospatial data when rendering cross-layer tile maps.

2.3.1. Scale Lifespan Variation Rule

The same geographic objects should conform to the change principle of scale decay from the high-level representation to the low one in the tile pyramid organization, which can be summarized as the scale lifespan variation rule [55].

According to the scaling sequence of cross-layer tile maps, the lake representation pattern is demonstrated as an instance. During the lifespan p_0 to p_n of the lake representation, a sequence basis state of the lake may be expressed in Equation (3). The entire lifespan of the lake may experience several scale transformations, denoted as ST_i , as presented in Equation (4). Figure 6 illustrates an example of the possible lifespan for the lake representation during cross-layer tile maps. The period p_0 to p_2 indicates the aggregation of neighboring lake clusters as a moderate variation while there is one abrupt change at time p_2 which is manifested in a river collapse with a bilinear lake branch into a single line. Immediately afterward, the single lake branch disappears at time p_3 , which may be regarded as another abrupt change. However, the simplification of the lake boundary from the period p_4 to p_5 is moderate and the same as the aggregation of three lake clusters at period p_5 . Finally, the elimination of the whole lake completely at time p_6 can be considered the last abrupt change during the lake lifespan representation.

$$\sum_{p_0}^{p_n} s_i = \{s_0, s_1, s_2, \dots, s_n\} \tag{3}$$

$$ST_i = \{G_i, [p_0, p_n], \sum_{p_0}^{p_n} s_i\} \tag{4}$$

where G_i is the scaling operation during the whole lifespan, which contains aggregation, collapse, simplification, and elimination.

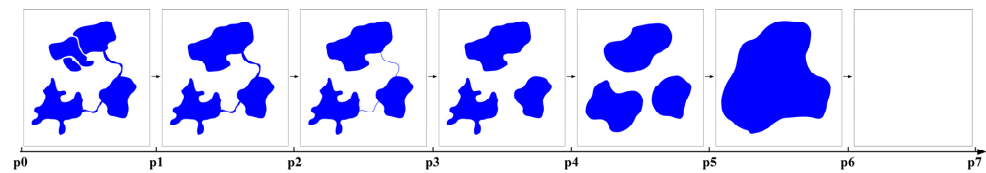


Figure 6. The lifespan of the lake representation in cross-layer tile maps.

Based on these principles, the sequence basis state forms and their corresponding scaling constraints are supposed to be expressed with the scale lifespan variation rule when rendering during the cross-layer tile map. The details are shown in Table 1. It is worth paying attention to the representation form change that desirably happened on the cross-layer base-state results following the tile display resolution. For example, forest land whose area is less than 9 mm^2 on the map needs to be eliminated, and buildings whose distance is less than 0.2 mm have to be aggregated.

Table 1. The scale lifespan variation rule of cross-layer tile maps.

Period	Situation	Rule Type	Change Type
1	Adjacent positions	Rule1 : $ST_1 = \{G_1 = \{\text{aggregation}\}, [s_i, s_j], \{\text{Object}_1\}\}$	Moderate change
2	Geometric dimension	Rule2 : $ST_2 = \{G_2 = \{\text{collapse}\}, [s_i, s_j], \{\text{Object}_2\}\}$	Abrupt change
3	Structural features	Rule3 : $ST_3 = \{G_3 = \{\text{simplification}\}, [s_i, s_j], \{\text{Object}_3\}\}$	Moderate change
4	Disappearance	Rule4 : $ST_4 = \{G_4 = \{\text{elimination}\}, [s_i, 0], \{\text{Object}_4\}\}$	Abrupt change

2.3.2. Geometric Consistency Rules

The global or local features of the same geographical objects under different representation levels are supposed to preserve certain geometric similarity, i.e., geometric consistency rules. Two feature indicators, the area variation degree (AVD) and the cross-layer consistency degree (CCD), are adopted in this context.

Area variation degree

The indicator AVD in inconsistency detection is calculated for the area change before and after the cross-layer rendering, which is shown in Equation (5).

$$AVD = \frac{|Area_{after} - Area_{before}|}{Area_{before}} \quad (5)$$

where $Area_{before}$ and $Area_{after}$ represent the total area of geographic objects in the cross-layer tile maps before and after rendering, respectively. The usual value range of the AVD is from 0 to 0.2. If $AVD = 0$. It means that the rendering is consistent, whereas if AVD exceeds 0.2, it means that there is a larger inconsistency after cross-layer map rendering.

Cross-layer consistency degree

The cross-layer consistency degree (CCD) can be obtained from the global feature consistency G and local feature consistency L with Equation (6). Specifically, the global feature consistency G before and after cross-layer tile map rendering is defined here by one hashing algorithm [56], as shown in Equation (7). Meanwhile, the local feature consistency L is provided by scale-invariant feature transform (SIFT) features [57,58]. The value ranges of CCD for cross-layer tile maps may be referred to in Table 2.

$$CCD = \mu \times G + \sigma \times L \quad (6)$$

$$G = \begin{cases} \frac{10-Hash}{10}, & Hash \leq 10 \\ 0, & Hash > 10 \end{cases} \quad (7)$$

where μ and σ are weighting coefficients, respectively, and $\mu + \sigma = 1$. In this study, the weighting coefficients are set to $\mu = \sigma = 0.5$. The value range of G is from 0 to 1. As the value of G increases, the consistency of the global features increases.

Table 2. The cross-layer consistency degree rule.

Value Range	$0 \leq CCD \leq 0.2$	$0.2 < CCD \leq 0.4$	$0.4 \leq CCD \leq 0.6$	$0.6 \leq CCD \leq 0.8$	$0.8 < CCD \leq 1.0$
Geometric consistency	Inconsistent	Less consistent	Moderately consistent	Highly consistent	Exactly consistent

2.4. Data Scaling and Derivation with Super-Pixel Segmentation

The two-level tile map data representation from $Level_i$ to $Level_{i+1}$ is an explicit process of decaying representation in the scale lifespan. When judging whether the rendering results of these two levels are consistent, an initial representation result $Level'_i$ can be obtained through super-pixel processing for decaying the scale transformation of $Level_i$. Then, the difference between $Level'_i$ and $Level_{i+1}$ is matched, and when the discrepancy exceeds the limit, it may be considered inconsistent. In this evaluation, the scaling from $Level_i$ to $Level'_i$ is the pivotal task, so four operations are defined based on the super-pixel: aggregation, collapse, simplification, and elimination.

2.4.1. Aggregation

The cartographic distance between neighboring lakes or vegetation may decrease when the scale of the web map is reduced. In this case, the neighboring objects can

be appropriately aggregated to represent their overall characteristics. The process of neighboring water or vegetation area aggregation with super-pixels mainly includes three steps: super-pixel segmentation, the classification and selection of super-pixels, global aggregation, and local adjustment.

First, the simple linear iterative clustering (SLIC) algorithm [59] was utilized for planar water or vegetation area segmentation, resulting in five types of super-pixels from A to E, as displayed in Figure 7c. Type A super-pixels constitute the original planar geographic polygons, as shown in blue, while type B super-pixels with yellow are those external super-pixels which are the first order adjacent to type A super-pixels, and they are connected to only one polygon. Moreover, type C super-pixels are also the first order adjacent to type A super-pixels but these super-pixels are usually connected to two or more polygons, as displayed in orange. The dark yellow type D super-pixels commonly locate inside the planar objects of type A super-pixels. Except for the above four types of super-pixels, all the remaining super-pixels are type E super-pixels, as shown in white.

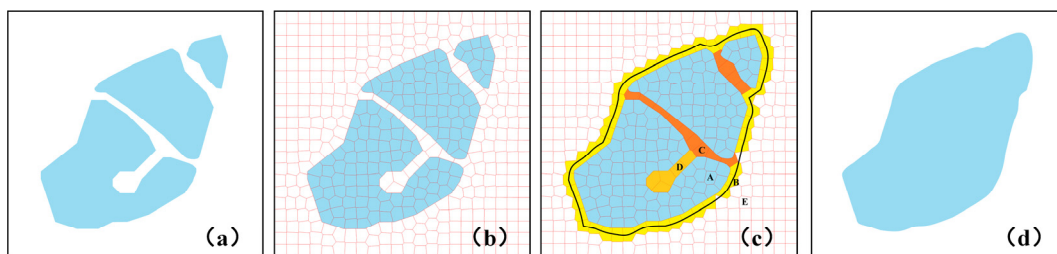


Figure 7. The lake aggregation with the super-pixel: (a) original data; (b) super-pixel segmentation by SLIC; (c) the classification and selection of different super-pixels; (d) the result of aggregation.

Second, the following selection and processing rules of super-pixels are defined to aggregate the planar clusters: (1) replace all super-pixels of type C and D to type A super-pixels; (2) select the center points of type B super-pixels in turn and connect them one by one to establish the initial boundary after global aggregation; and (3) local adjustment of the initial boundary is implemented by dilating, eroding, or smoothing operations.

2.4.2. Collapse

The process of collapse aims to deal with bilinear rivers that will be converted into one single-line river after cross-layer tile map rendering. Moreover, it is typically composed of two primary procedures: segmentation, centerline extraction, and smoothing.

At first, the bilinear river was segmented with the SLIC algorithm to generate two types of super-pixels, A and B, which are presented in Figure 8b. Type A super-pixels, which are shown in blue, make up the original river, while the others are type B super-pixels, as displayed in white. Thus, the collapse rules are described as follows: (1) extract and connect the center points in turn of the type A super-pixels and the head and tail ends of this river to derive one centerline; (2) smoothing the centerline with the morphological operations.

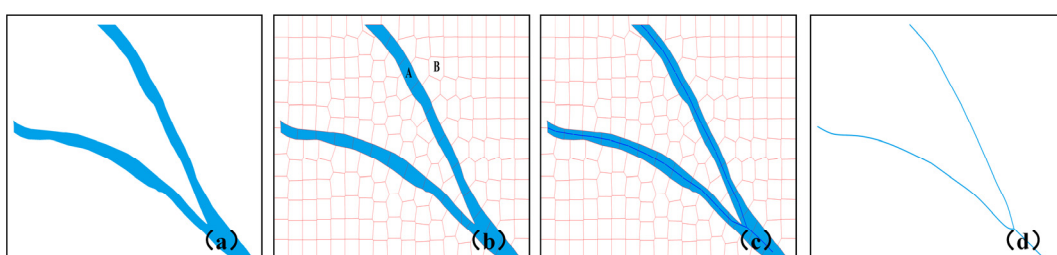


Figure 8. The collapse of bilinear river with the super-pixel: (a) original data; (b) super-pixel segmentation by SLIC; (c) the centerline extraction from the super-pixels; (d) the result of collapse.

2.4.3. Simplification

The most prominent purpose of geospatial data simplification in web maps is to remove the details of planar contour shapes, thus maintaining their global features. In the cross-layer tile map, four major procedures are covered in the water or vegetation boundary simplification under super-pixel structure: segmentation, the classification and selection of super-pixels, bending processing, and local adjustment.

The SLIC algorithm is employed again for planar object segmentation to form four types of super-pixels from A to D, which are demonstrated in Figure 9b: (1) type A super-pixels, which are presented in blue, locate inside the closed planar region and do not intersect with the boundary; (2) the pink type B super-pixels are within the closed planar region and intersect the boundary; (3) the position of the gray type C super-pixels are outside the enclosed planar area and they intersect the boundary; and (4) the remaining type D super-pixels, which are shown in white, are located outside the closed planar area and also do not intersect the boundary.

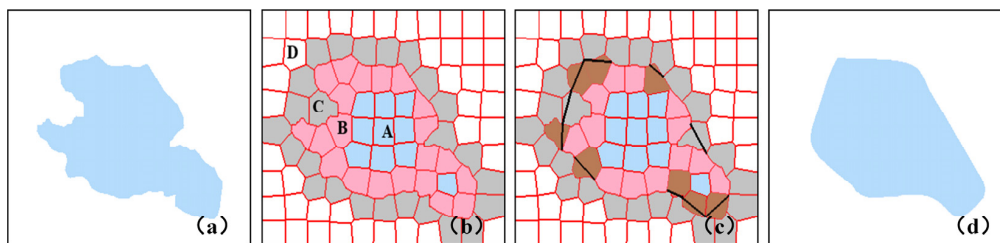


Figure 9. The simplification with the super-pixel: (a) original data; (b) super-pixel segmentation and the classification by SLIC; (c) the selection and the bend smooth from different super-pixels; (d) the result of simplification.

The super-pixel selection and boundary simplification rules are adopted as follows: (1) select types B and C super-pixels and connect the endpoints between the super-pixels whose boundaries are to be simplified; (2) sharpen the convex bend or fill the concave bend, e.g., the brown type B super-pixels; and (3) smooth the connected edges using Fourier descriptors [60].

2.4.4. Elimination

When the geographic objects of a tile map are scaled down to a certain level, causing the objects to be too small or too narrow to be represented on the map, it is necessary to eliminate them from the tile map. The elimination mainly directly deletes the two small blue super-pixels A1 and A2, which are displayed in Figure 10c from the tile map in the context of consistency rendering rules.

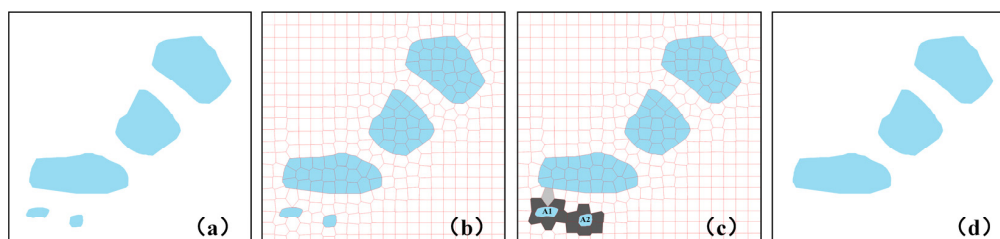


Figure 10. The elimination of small areas with the super-pixel: (a) original data; (b) super-pixel segmentation by SLIC; (c) the classification and selection of small areas; (d) the result of elimination.

2.5. Inconsistency Detection for Cross-Layer Tile Maps

Directly overlaying two different layer tile maps to analyze the inconsistency of geographic objects inevitably leads to misjudgment or omission. Hence, three aspects in this study are perceived and summarized for inconsistency detection of cross-layer tile maps,

namely, inconsistency sources, inconsistency classifications, and overlay analysis of inconsistency. The cross-layer tile map inconsistency information perception and classification are presented in Figure 11 and Table 3.

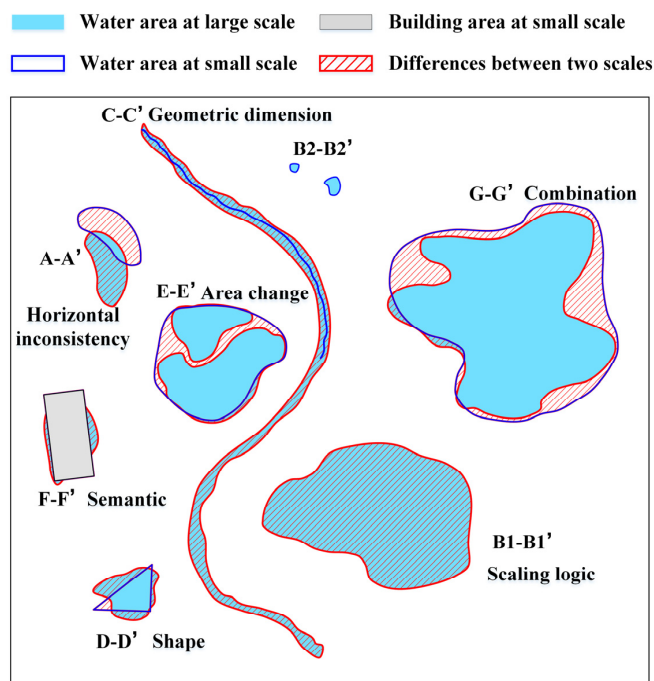


Figure 11. Examples of water area differences in cross-layer tile map.

Table 3. The cross-layer tile map inconsistency detection references.

Information	Type	Performance	Example in Figure 10	Judgment Basis
Inconsistency sources	Horizontal inconsistency	Inconsistent location in tile levels	A-A'	/
	Vertical inconsistency	Inconsistent representation by map generalization	E-E' G-G'	Scale lifespan variation rule
Inconsistency classifications	Scaling logic	Contrary to the actual scale change requirement	B1-B1' B2-B2'	Scale lifespan variation rule
	Geometric dimension	Bilinear, single-line, dot representation disorder	C-C'	Scale lifespan variation rule
	Shape	Irregularity of the boundary	D-D'	Scale lifespan variation rule or cross-layer consistency degree
	Area change	Area change by map generalization	E-E'	Area variation degree
	Semantic	Change of object type	F-F'	/
	Combination	Any two or more inconsistencies	G-G'	All consistency rendering rules

From the perspective of the strategy for cross-layer tile map rendering, it is first necessary to distinguish between horizontal and vertical inconsistency based on the origin change-associated objects. The former is manifested in Figure 11 (A-A') by geographical locations due to different coordinate or projection transformations, while the latter is usually a different representation resulting from cartographic generalization, such as in Figure 11 (E-E' and G-G'). In the case of the water tile map in Figure 11, the inconsistent information mainly occurs from geometric dimension, graphical shape, and area changes, including the unfinished collapse from the bilinear river to a single-line river (C-C'), the original smooth lake shape into a triangle (D-D'), and the area change after the aggregation of neighboring lakes (E-E'). In addition, the violation of the scaling logic in which small lakes

(B2-B2') are not deleted while the large lake (B1-B1') suddenly disappears also deserves concern. Moreover, there are also semantic inconsistencies such as waters turning into buildings after rendering (F-F'), which are not temporarily considered in the study. The above-referred situations may be detected by the consistency rendering rules for cross-layer tile maps described in Section 2.3.

Based on this, the cross-layer tile map inconsistency detection is performed with the support of overlapping operation analysis, and the specific process is as follows. First, a new small-scale rendering result $Level'_i$ map tile is initially derived from certain large-scale map tiles with $Level_i$ based on a super-pixel scaling process. Then, the two layers $Level'_i$ and $Level_{i+1}$ are overlapped together to obtain the discrepancy layer information by logical intersection, union, and difference operations. The logical intersection and logical difference can be implemented in GIS software employing the Intersect and Erase operators, respectively. Finally, the cross-layer data inconsistency region is acquired under the guidance of cross-layer tile map inconsistency detection knowledge. The inconsistent information may be filtered by evaluating the significance of logical differences. In this study, the cross-layer inconsistency is considered when the value of the difference between the two layers $Level'_i$ and $Level_{i+1}$ exceeds 0.2.

3. Results

3.1. Separation Results

Figure 12 displayed the object extraction results for the water and vegetation areas at different levels of the tile map by utilizing the method in Section 2.2, where the color of water corresponds to RGB = (194, 223, 255) and the vegetation color corresponds to RGB = (197, 240, 220). It is essential to mention that the actual water and vegetation in the test area may be slightly smaller than the original experimental area due to the fact that only paired data that match the cross-layer range can be applied to the test of inconsistency detection.

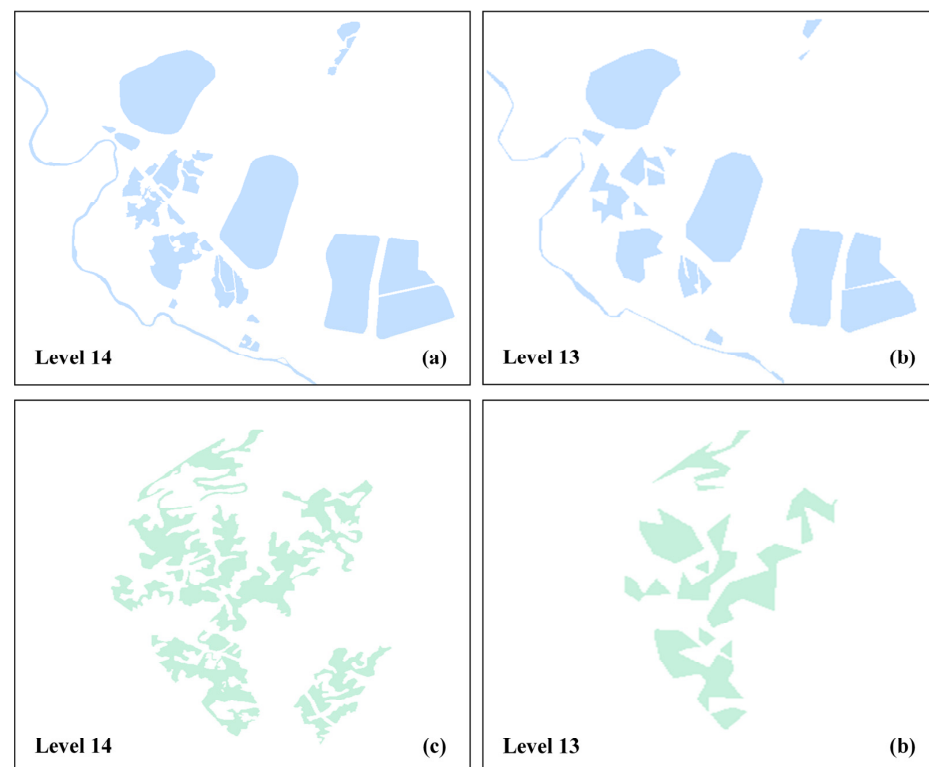


Figure 12. Object separation results of water and vegetation areas at different levels of tile maps: (a,b) display water areas, while (c,d) show vegetation areas at Level 14 and Level 13, respectively.

It can be observed as follows: the threshold segmentation from two colors in Section 2.2 can reasonably allow the separation of geographic objects in the region at the global hierarchy, while at the local horizon, the related morphological operations provide the benefits to complement and connect the gap problems due to place names, roads, or other map symbols. Consequently, the visual representation of its image is a complete planar result. Therefore, the user can efficiently obtain different types of geographic objects directly with raster images from the cross-layer tile map through the method in Section 2.2.

3.2. Inconsistency Detection

Based on the proposed CRTMRM, planar water and vegetation areas from the Baidu map are relatively well applied. Meanwhile, the aggregation, collapse, simplification, and elimination strategies under the super-pixel grid are adopted when scaling with consistency rendering rules for cross-layer tile maps. Thus, the inconsistency detection and post-rendering results of water and vegetation from Level 14 to Level 13 are visualized by cross-layer tile maps.

3.2.1. Visualization Results

The parameters of the CRTMRM employed on the Level 14 tile maps of this study are described in Table 4, and their specific meanings are as follows. S_1 is the size of super-pixels for clustering based on the SLIC algorithm for lakes or vegetation, while S_2 is the size of super-pixels mainly for narrow bilinear river areas. When setting parameters S_1 and S_2 , it is recommended to follow Töpfer's radical law [61]. The minimum distance d indicates the need to aggregate neighboring map objects, and *Area* represents the number of pixels of all polygon objects in the test area except for rivers. In this study, the following two formulas for selecting the size of super-pixel segmentation are referred to:

$$\frac{scale_o}{scale_t} = \left(\frac{N_o}{N_t} \right)^2, s_1 = N_t \quad (8)$$

$$w_b^2 < w < w_a^2, s_2 = \sqrt{w} \quad (9)$$

where $scale_o$ and $scale_t$ are the denominators of the original and target map scales respectively, the specific ratio result is 1/2; N_o denotes the size of map pixels at the original scale, whose value is 16 here; N_t represents the size of the ideal super-pixel segmentation, whose value is about 23 here. In addition, w_a and w_b , are the number of pixels at the widest and narrowest parts of the river, respectively, and w is the ideal super-pixel segmentation size of the river. The values of these parameters are defined in pixels and are not fixed, but are relatively reasonable in this experiment, as shown in Table 3, where the symbol “/” indicates that the corresponding method does not include the parameter.

Table 4. Parameters related to scaling in this study.

Category	Level	S_1	S_2	d	Area
Water	14	20	8	40 m	91,945
Vegetation	14	25	/	40 m	31,583

The results of the inconsistency detection of water and vegetation data from the cross-layer tile map are demonstrated in Figure 13. Primarily, it can be viewed that the proposed CRTMRM enables the effective derivation of lake and river or vegetation results across scales in tile maps. As shown in Figure 13a, more neighboring lake clusters that should be merged into a whole have been aggregated at Level 13' and derived after scaling with the super-pixel. Moreover, the global morphological features of lakes after aggregation can be effectively maintained. Furthermore, those small area lakes that were not eliminated have been also successfully detected and deleted. In addition, one narrow bilinear river that should be converted to a single-line river is detected while the derived single-line river is still consistent

with the original bilinear river trend and boundary. Meanwhile, the shape of the lake with too straight boundary has been found and then smoothed, as well as its global and local features have been preserved. In contrast, in Figure 13c, the vegetation areas with concentrated distribution and irregular shape are mainly aggregated and simplified one by one within the constraints of the scale lifespan variation rule. It is mainly manifested in the reduction of the number of vegetation polygons and the smoothness of their contour boundaries.

During the inconsistency detection for two cross-layer tile maps, the most apparent result is the vertical inconsistency from cartographic generalization according to the scale lifespan variation rule. Specifically, the narrow river at Level 13 from the Baidu map in Figure 13b was not rendered about collapse, which led to the difference of geospatial data in cross-layer representation. Furthermore, the vegetation in the lower right corner of Figure 13d is not only not aggregated, but even directly eliminated, which may substantially contribute to the cognitive mistakes of the map users about this area.

To gain a better insight into the characteristics of the CRTMRM in detecting inconsistencies from cross-layer tile maps, as presented in Figure 14, some typical places were magnified for comparison. The three images on the left are visualization results of water areas while the right three images are vegetation areas. As illustrated in these pictures, the rendering results of the water and vegetation area from the CRTMRM are effective in maintaining the overall characteristics during cross-layer tile maps.

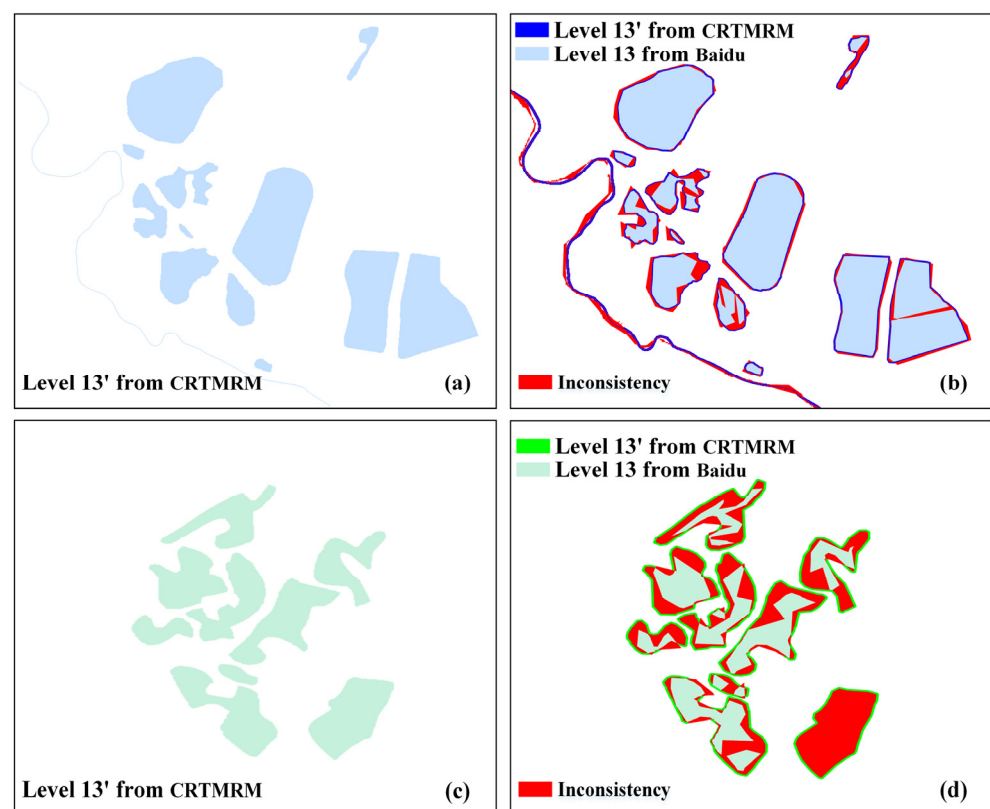


Figure 13. Water and vegetation data derivation and inconsistency detection for cross-layer tile maps. (a,c) are water and vegetation at Level 13' from CRTMRM, respectively. (b,d) are the comparison results.

On the one hand, in the case where a bilinear river is supposed to be converted into a single-line river, as marked by the red circles from Figure 14a–c, the bilinear river is typically expected to satisfy the scale lifespan variation rule for collapse during the map rendering from Level 14 to Level 13. At this point, it belongs to the combination inconsistency of scaling logic and geometric dimension. The CRTMRM derives a more reasonable rendering result while detecting this inconsistency from the cross-layer map caused by the fractured river and with no collapse scenarios in the Baidu map. In addition, the shape inconsistency

was detected as highlighted by the purple circle in Figure 14b. The visualization of rougher boundaries or sharp corners for the lake at Level 13 is not optimal. Similarly, the green circle in Figure 14a would be attributed to a combination inconsistency because neighboring lakes needing aggregation were simplified into a small triangle with the green mark in Figure 14b. Therefore, while reasonably aggregating the lakes, the global morphological characteristics of the neighboring lake groups before and after aggregation were basically maintained from the CRTMRM, which may also provide a foundation for the inconsistency detection. However, this also brings the effect of increasing the area with it. Inevitably, this may also bring the drawback of area increase with it.

On the other hand, for the visualization of vegetation from Level 14 to Level 13, as indicated by the blue circles from Figure 14d–f, a large area of vegetation was not aggregated or simplified according to the consistency rendering rules for cross-layer tile maps but was obviously deleted by mistake. Moreover, the two vegetation polygons with yellow circles in Figure 14d, which ought to be aggregated due to their proximity, were visualized as two isolated polygons in Figure 14e, which might be regarded as a combination inconsistency of scaling logic and shape.

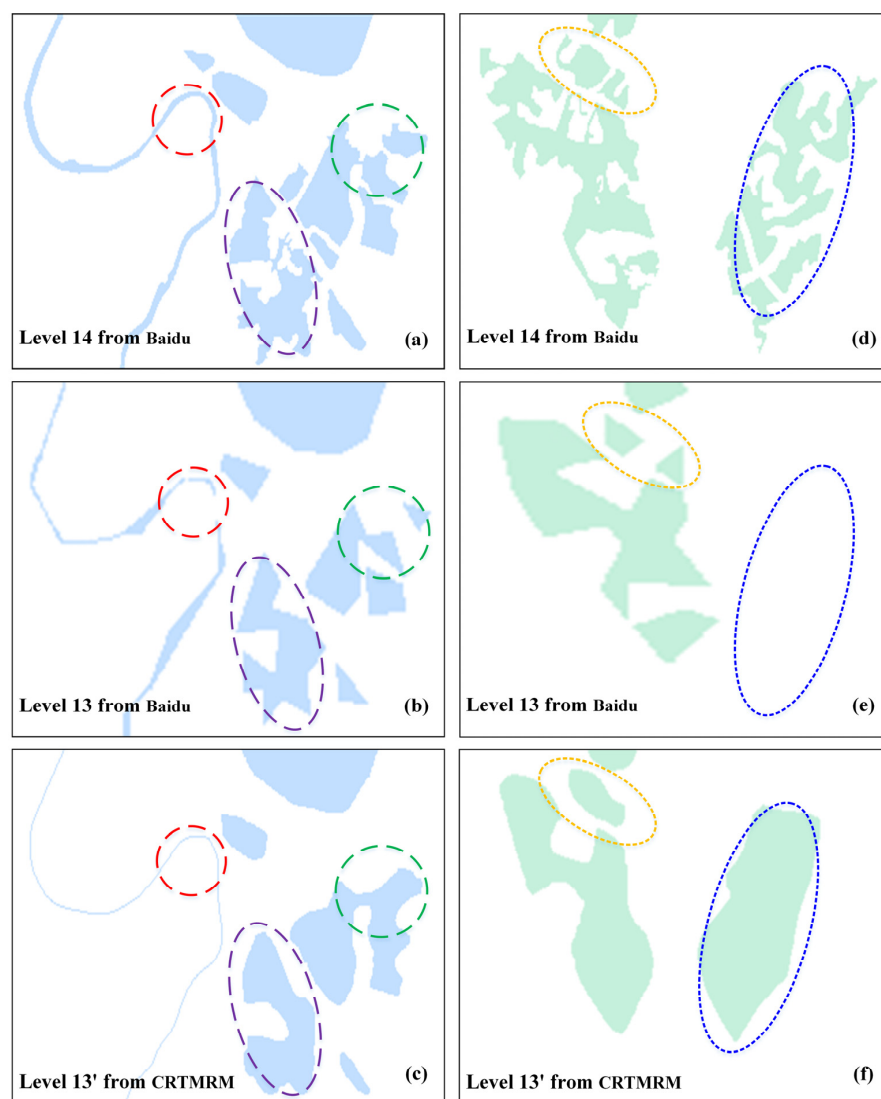


Figure 14. The details of rendering visualization between two tile map comparisons. (a–c) represents different rendering results of water data while (d–f) shows different rendering results of vegetation data.

3.2.2. Indicator Performance

The area variation degree (AVD) and the cross-layer consistency degree (CCD) were selected to statistically compare the characteristics of the two rendering visualization results from cross-layer tile maps. Table 5 contains some values related to the AVD of water and vegetation at Level 13 from the Baidu map and Level 13' from the CRTMRM.

Table 5. The number and area characteristics of two rendering visualization results.

Type	Method	Original Numbers	Numbers after Processing	Number Change Rate	Area after Processing	AVD	Numbers of Rivers after Processing	Maximum River Width after Processing
Water	Baidu map	26	17	0.346	84,676	0.079	2	7
	CRTMRM	26	12	0.538	86,379	0.061	1	1
Vegetation	Baidu map	14	11	0.214	12,226	0.613	/	/
	CRTMRM	14	9	0.357	43,685	0.383	/	/

According to the results in the table, the overall number of objects after cross-layer rendering is similar for both water and vegetation areas. However, the number change rate of the CRTMRM is relatively larger than that of the Baidu map visualization, which is because more neighboring lakes or vegetation are more consistently processed for aggregation and simplification in Figure 14c due to the constraint of consistency rendering rules for cross-layer tile maps.

Nevertheless, in terms of the actual area variation degree, the two rendering methods are relatively similar in their performance in the water area, both around 0.07. Whereas, there is an area variation degree of more than 0.6, which greatly exceeds the CRTMRM in the vegetation area of the Baidu map, simply on account of the lack of the range marked by the blue circles in Figure 14e. This region may be recognized as an obvious manifestation of geospatial data inconsistency after the cross-layer tile map rendering. Furthermore, a matter worthy of attention is the data inconsistency issue in narrow rivers. Compared with the CRTMRM, the number of rivers in the Baidu map increases, and the maximum width of rivers is seven pixels after cross-layer rendering, which is due to a river disruption. The specific visualization results can also be found in the red circles from Figure 14a–c.

The performance of two rendering visualizations, Level 13 from the Baidu map and Level 13' from the CRTMRM, was evaluated utilizing the cross-layer consistency degree (CCD), and their similarity to Level 14 is presented in Table 6. In terms of global consistency similarity, the value results at Level 13 from the Baidu map are unsatisfactory, with both the water and vegetation test areas below 0.5, indicating a major cross-layer tile map data inconsistency in the region. The CRTMRM, instead, remains above 0.8 for the value of global consistency similarity in the region, so it would be able to serve as a tool to assist cross-layer tile map inconsistency detection in terms of global features to some extent.

Table 6. The geometric characteristics of two rendering visualization results.

Type	Method	G	L	CCD
Water	Baidu map	0.400	0.582	0.491
	CRTMRM	0.900	0.610	0.755
Vegetation	Baidu map	0.300	0.587	0.444
	CRTMRM	0.800	0.568	0.684

As for local consistency results, two rendering visualization results of both water and vegetation areas are not very different, basically remaining around 0.58. In the vegetation area, the local feature consistency from the Baidu map reaches about 0.587, which is slightly better than that of the CRTMRM. This is partly due to the fact that the boundaries of

vegetation polygons after aggregation and simplification from the CRTMRM may lead to slightly fewer key points in SIFT matching than the Baidu map rendering result. However, judging from the values of the CCD, the data consistency at Level 13' derived from the CRTMRM all remain above 0.68, whose values are all higher than the Baidu map. Thus, the rendering results from the CRTMRM may be considered as one basic comparative data for cross-layer tile maps to facilitate the task of inconsistency detection.

4. Discussion

The feasibility and universality of the CRTMRM for other web map renderings are explored, and the future direction of the super-pixel-based scaling method for tile map inconsistency detection or rendering is presented.

4.1. The Availability and Universality of the CRTMRM

The CRTMRM provides a demonstrative manifestation in cross-layer tile map inconsistency detection. Moreover, a data structure with super-pixel and processing strategy for raster cross-layer map rendering is established. It is feasible to directly implement the scaling of tile maps in raster form from a super-pixel perspective for users. Moreover, the comparison and analysis of raster tile map objects are possible to be accomplished, which supports inconsistency detection from cross-layer changes in web map rendering. In this way, the bottleneck that the vector structure inconsistency detection or processing cannot be directly applied to multi-level raster tile maps may be partly resolved.

Furthermore, to demonstrate the availability of the proposed CRTMRM when applied in other web maps, the test areas of two other web maps, the Amap and Google map, were employed for display as follows. Figure 15a,b represents two raw tile images covering vegetation areas at Level 10 and Level 9 of the Amap, while Figure 15d,e shows two water areas at Level 12 and Level 10 from the Google map. Subsequently, the results of the cross-layer tile map inconsistency detection for water and vegetation from two different web maps were depicted in Figure 15c,f. Some characteristics could be derived from it, with the following details:

(1) The proposed CRTMRM may be feasible and available with regard to its ability to efficiently implement the processing for different web maps, such as Amap and Google Maps directly from the map tiles in pixel form.

(2) In the derivation process of cross-layer tile maps, the lake and vegetation distribution features may be preserved at different levels as the map scale decreases.

(3) The amount of vegetation at Level 9 from the Amap and at Level 9' from the CRTMRM are five and two, respectively, which are all less than the number of vegetation visualized at Level 10. Meanwhile, the vegetation results rendering from the Amap are quite different, as indicated through the purple arrows in Figure 15c. Hence, it may be considered a combination inconsistency of scaling logic and area change across layers in this region.

(4) The amount of water at Level 10' from the CRTMRM is far less than that at Level 10 from the Google map. Moreover, the difference between Level 10 and Level 12 of the Google map is extremely small. This is partly a consequence of the failure to follow the scale lifespan variation rule for water areas when displayed across levels.

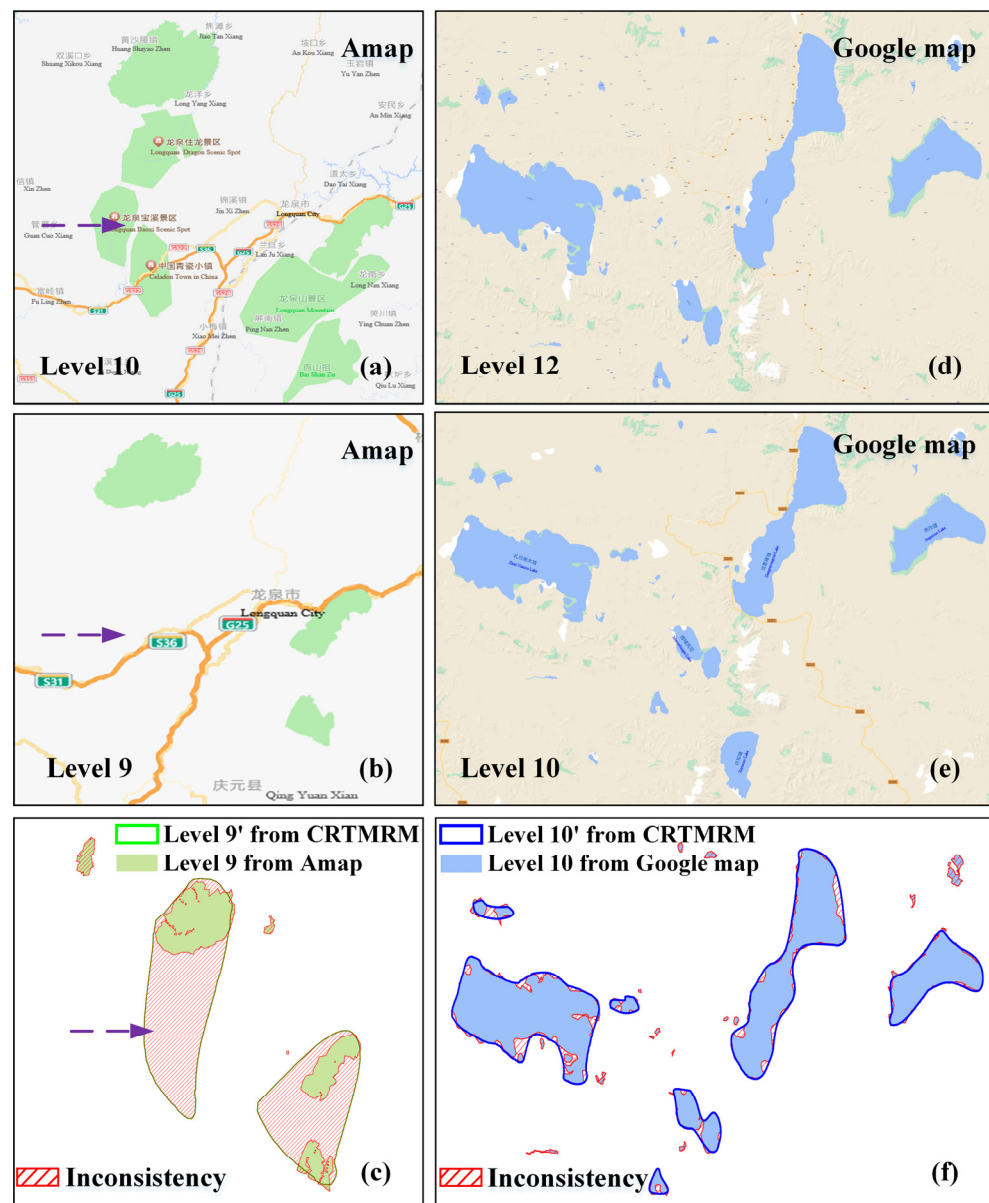


Figure 15. Data inconsistency detection for Amap and Google map tiles. (a–c) represents inconsistent areas of vegetation in Amap while (d–f) shows inconsistent areas of water in Google map.

4.2. Some Future Directions for Inconsistency Detection from Cross-Layer Tile Maps

The consistency between geospatial data in web maps is of great significance for intelligent urban construction and collaborative data processing. The framework of cross-layer raster tile map rendering is primarily to detect the inconsistency between tile maps across levels. With the pixel raster model, it is possible to straightly analyze and detect geospatial data inconsistencies from cross-layer web map tiles through the vertical feedback of the scale lifespan variation rule of geographic objects and the horizontal feedback of geometric consistency rules.

Unlike the vector inconsistency detection that relies on the regional features and matching relationship, the CRTMRM reveals the intrinsic mechanism of cross-scale geographic objects of tile maps representation at the pixel level. However, there are still some limitations in this study. First, the tile map scaling requires a manual setting of ideally reasonable parameter values, which can be further developed in the direction of automated processing technology techniques in the future. Second, the inconsistency detection of single polygon geospatial data of tile maps, such as water or vegetation, was chiefly taken into account in

the CRTMRM, but it lacks the detection of point and line type geospatial data. In addition, it is still a challenge to completely solve the various data layers or multi-object collaboration in different environments due to the complicated spatial relationships.

In the future, in the data inconsistency detection of cross-layer tile maps, it is necessary to further understand and analyze the interrelated rules of geometric, semantic, and spatial relation from multi-source geographic objects, and enhance the automation of detection methods. In addition, some priori rules of cross-layer geospatial data variation can be introduced as the basis of inconsistency detection, such as the selection or discard of famous scenic spots, and the scale variation patterns of the main streams and tributaries of rivers. Moreover, it is essential to comprehensively construct an integrated system for detecting the inconsistency between geospatial data from multi-source and multi-scale tile maps in point-line-polygon mode. The raster structure segmentation scaling model may also be extended for the processing of multiple geographic objects or complex scenes. In this way, it may quickly detect the changes in geographic objects in the web map and provide a foundation for realizing the geospatial data updating.

5. Conclusions

The consistency of cross-layer geospatial data is of vital significance for the integration, fusion, updating, and application of geographic information in web maps. In this study, a framework called the CRTMRM for detecting inconsistencies between cross-layer tile map geospatial data utilizing a raster-based scaling method is demonstrated. In accordance with the scale lifespan variation and geometric consistency rules, the reference cross-layer rendering map results may be derived from a super-pixel segmentation-based approach. In addition, a set of processes supporting the inconsistency detection of geospatial data across hierarchical web maps has been established and it contributes substantially to the in-depth analysis and rendering of web maps. Compared with traditional vector matching and detection inconsistency methods, the advantages of tile map processing in raster mode, super-pixel segmentation in the application when scaling, and cross-layer data consistency comparison has been integrated into the CRTMRM. Furthermore, it facilitates map users to perceive geospatial data or multi-source web objects directly from pixel-represented map tiles.

Specifically, the planar water or vegetation data inconsistency from Level 9 to 14 with Baidu Maps, Amap, and Google Maps are all well detected by the CRTMRM. In terms of preserving global and local feature consistency across levels of geospatial data, the reference data after cross-layer rendering via the CRTMRM can effectively perform direct elimination of small water or vegetation areas. Meanwhile, neighboring lakes or vegetation groups can be successfully aggregated, and narrow rivers may be collapsed. On this basis, it is also capable to well maintain the features such as global patterns or boundary smoothing after rendering. In addition, data inconsistencies inherently represented across scales in geospatial data of web maps may be effectively detected by a deep understanding of mechanisms among cross-layer tile maps based on geographic laws and visual cognition, such as the sudden disappearance of vegetation and fractured rivers.

In general, the super-pixel data structure and processing strategy for unstructured cross-layer web map rendering is demonstrated through the CRTMRM and it has a good exemplary representation in facilitating cross-layer tile map inconsistency detection, but there are still some points that deserve further exploration. The semantic, and spatial-relation inconsistency detection should also be regarded to optimize the framework. In the future, a multi-scale tile map geospatial data inconsistency detection system with a point-line-polygon model should be implemented to directly perform unstructured web map data inconsistency detection and provide new methodological support for the development of intelligent web map mapping.

Author Contributions: Conceptualization, Junbo Yu and Tinghua Ai; methodology, Junbo Yu and Yilang Shen; validation, Junbo Yu, Haijiang Xu and Lingrui Yan; formal analysis, Junbo Yu and Haijiang Xu; investigation, Junbo Yu; data curation, Lingrui Yan; writing—original draft preparation, Junbo Yu; writing—review and editing, Junbo Yu, Tinghua Ai and Haijiang Xu; visualization, Junbo

Yu and Lingrui Yan; supervision, Tinghua Ai; funding acquisition, Yilang Shen. All authors have read and agreed to the published version of the manuscript.

Funding: This research was funded by the National Natural Science Foundation of China, grant numbers 42001402 and 42271454.

Data Availability Statement: The raw tile maps can be obtained from the URL services of Baidu Maps, Amap, and Google Maps. The test tile data in this study can be downloaded from <https://doi.org/10.6084/m9.figshare.22269037.v1>, accessed on 14 March 2023.

Acknowledgments: Special thanks are given to the editor and reviewers for their suggestions.

Conflicts of Interest: The authors declare no conflict of interest.

References

- Kouvelas, A.; Aboudolas, K.; Papageorgiou, M.; Kosmatopoulos, E.B. A Hybrid Strategy for Real-Time Traffic Signal Control of Urban Road Networks. *IEEE Trans. Intell. Transp. Syst.* **2011**, *12*, 884–894. [\[CrossRef\]](#)
- Biljecki, F.; Ito, K. Street view imagery in urban analytics and GIS: A review. *Landsc. Urban Plan.* **2021**, *215*, 104217. [\[CrossRef\]](#)
- Ohno, K.; Nomura, T.; Tadokoro, S. Real-Time Robot Trajectory Estimation and 3D Map Construction using 3D Camera. In Proceedings of the 2006 IEEE/RSJ International Conference on Intelligent Robots and Systems, Beijing, China, 9–15 October 2006; pp. 5279–5285.
- Nurminen, A. Mobile 3D City Maps. *IEEE Comput. Graph. Appl.* **2008**, *28*, 20–31. [\[CrossRef\]](#)
- Mi, X.; Yang, B.; Dong, Z.; Liu, C.; Zong, Z.; Yuan, Z. A two-stage approach for road marking extraction and modeling using MLS point clouds. *ISPRS J. Photogramm. Remote Sens.* **2021**, *180*, 255–268. [\[CrossRef\]](#)
- Ballatore, A.; Bertolotto, M.; Wilson, D.C. Geographic knowledge extraction and semantic similarity in OpenStreetMap. *Knowl. Inf. Syst.* **2013**, *37*, 61–81. [\[CrossRef\]](#)
- Xu, F.F.; Lin, B.Y.; Lu, Q.; Huang, Y.; Zhu, K.Q. Cross-region traffic prediction for China on OpenStreetMap. In Proceedings of the 9th ACM SIGSPATIAL International Workshop on Computational Transportation Science, Burlingame, CA, USA, 31 October–3 November 2016; pp. 37–42.
- García Martín, R.; de Castro Fernández, J.P.; Verdú Pérez, E.; Verdú Pérez, M.J.; Regueras Santos, L.M. An OLS regression model for context-aware tile prefetching in a web map cache. *Int. J. Geogr. Inf. Sci.* **2013**, *27*, 614–632. [\[CrossRef\]](#)
- Xiao, Y.; Ai, T.; Yang, M.; Zhang, X. A Multi-Scale Representation of Point-of-Interest (POI) Features in Indoor Map Visualization. *ISPRS Int. J. Geo-Inf.* **2020**, *9*, 239. [\[CrossRef\]](#)
- Antoniou, V.; Morley, J.; Haklay, M. Tiled Vectors: A Method for Vector Transmission over the Web. In Proceedings of the Web and Wireless Geographical Information Systems, Berlin/Heidelberg, Germany, 7–8 December 2009; pp. 56–71.
- Peterson, M.P. The Tile-Based Mapping Transition in Cartography. In *Maps for the Future: Children, Education and Internet*; Zentai, L., Reyes Nunez, J., Eds.; Springer: Berlin/Heidelberg, Germany, 2012; pp. 151–163.
- Netek, R.; Masopust, J.; Pavlicek, F.; Pechanec, V. Performance Testing on Vector vs. Raster Map Tiles—Comparative Study on Load Metrics. *ISPRS Int. J. Geo-Inf.* **2020**, *9*, 101. [\[CrossRef\]](#)
- McNeill, G.; Hale, S.A. Generating Tile Maps. *Comput. Graph. Forum* **2017**, *36*, 435–445. [\[CrossRef\]](#)
- Koen, E.L.; Ellington, E.H.; Bowman, J. Mapping landscape connectivity for large spatial extents. *Landsc. Ecol.* **2019**, *34*, 2421–2433. [\[CrossRef\]](#)
- Jenny, B.; Buddeberg, J.; Hoarau, C.; Liem, J. Plan oblique relief for web maps. *Cartogr. Geogr. Inf. Sci.* **2015**, *42*, 410–418. [\[CrossRef\]](#)
- Zhang, M.; Huang, H.; Li, Z.; Hackman, K.O.; Liu, C.; Andriamiarisoa, R.L.; Ny Aina Nomenjanahary Raherivelo, T.; Li, Y.; Gong, P. Automatic High-Resolution Land Cover Production in Madagascar Using Sentinel-2 Time Series, Tile-Based Image Classification and Google Earth Engine. *Remote Sens.* **2020**, *12*, 3663. [\[CrossRef\]](#)
- Goodchild, M.F.; Li, L. Assuring the quality of volunteered geographic information. *Spat. Stat.* **2012**, *1*, 110–120. [\[CrossRef\]](#)
- Even-Tzur, G. Invariance property of coordinate transformation. *J. Spat. Sci.* **2018**, *63*, 23–34. [\[CrossRef\]](#)
- Jenny, B.; Šavrič, B. Enhancing adaptive composite map projections: Wagner transformation between the Lambert azimuthal and the transverse cylindrical equal-area projections. *Cartogr. Geogr. Inf. Sci.* **2018**, *45*, 456–463. [\[CrossRef\]](#)
- Duan, W.; Chiang, Y.-Y.; Leyk, S.; Uhl, J.H.; Knoblock, C.A. Automatic alignment of contemporary vector data and georeferenced historical maps using reinforcement learning. *Int. J. Geogr. Inf. Sci.* **2020**, *34*, 824–849. [\[CrossRef\]](#)
- Wolter, D.; Blank, D.; Henrich, A. Georeferencing River Networks Using Spatial Reasoning. In Proceedings of the 11th Workshop on Geographic Information Retrieval, Heidelberg, Germany, 30 November–1 December 2017; p. 6.
- Sheeren, D.; Mustière, S.; Zucker, J.D. A data-mining approach for assessing consistency between multiple representations in spatial databases. *Int. J. Geogr. Inf. Sci.* **2009**, *23*, 961–992. [\[CrossRef\]](#)
- Karsznia, I.; Przychodzeń, M.; Sielicka, K. Methodology of the automatic generalization of buildings, road networks, forests and surface waters: A case study based on the Topographic Objects Database in Poland. *Geocarto Int.* **2020**, *35*, 735–758. [\[CrossRef\]](#)
- Qi, H.B.; Li, Z.L.; Chen, J. Automated change detection for updating settlements at smaller-scale maps from updated larger-scale maps. *J. Spat. Sci.* **2010**, *55*, 133–146. [\[CrossRef\]](#)

25. Yang, M.; Ai, T.; Yan, X.; Chen, Y.; Zhang, X. A map-algebra-based method for automatic change detection and spatial data updating across multiple scales. *Trans. GIS* **2018**, *22*, 435–454. [[CrossRef](#)]
26. Duckham, M.; Lingham, J.; Mason, K.; Worboys, M. Qualitative reasoning about consistency in geographic information. *Inf. Sci.* **2006**, *176*, 601–627. [[CrossRef](#)]
27. Ubeda, T.; Egenhofer, M.J. Topological error correcting in GIS. In Proceedings of the Advances in Spatial Databases, Berlin, Germany, 15–18 July 1997; pp. 281–297.
28. Xuan, L.; Shekhar, S.; Chawla, S. Consistency checking for Euclidean spatial constraints: A dimension graph approach. In Proceedings of the 12th IEEE International Conference on Tools with Artificial Intelligence, ICTAI 2000, Vancouver, BC, Canada, 15 November 2000; pp. 333–342.
29. Mara, S.; Mara, H.; Aktug, B.; Mara, E.; Yildiz, F. Topological error correction of GIS vector data. *Int. J. Phys. Sci.* **2010**, *5*, 476–483.
30. Du, S.; Qin, Q.; Wang, Q.; Ma, H. Evaluating structural and topological consistency of complex regions with broad boundaries in multi-resolution spatial databases. *Inf. Sci.* **2008**, *178*, 52–68. [[CrossRef](#)]
31. Du, S.; Guo, L.; Wang, Q. A scale-explicit model for checking directional consistency in multi-resolution spatial data. *Int. J. Geogr. Inf. Sci.* **2010**, *24*, 465–485. [[CrossRef](#)]
32. Li, W.; Zhu, J.; Fu, L.; Zhu, Q.; Xie, Y.; Hu, Y. An augmented representation method of debris flow scenes to improve public perception. *Int. J. Geogr. Inf. Sci.* **2021**, *35*, 1521–1544. [[CrossRef](#)]
33. Li, W.; Raskin, R.; Goodchild, M.F. Semantic similarity measurement based on knowledge mining: An artificial neural net approach. *Int. J. Geogr. Inf. Sci.* **2012**, *26*, 1415–1435. [[CrossRef](#)]
34. Ruiz-Lendínez, J.J.; Ureña-Cámara, M.A.; Ariza-López, F.J. A Polygon and Point-Based Approach to Matching Geospatial Features. *ISPRS Int. J. Geo-Inf.* **2017**, *6*, 399. [[CrossRef](#)]
35. Yi, S. Learning ontologies for geographic entity matching and multi-sources data fusion. In Proceedings of the 2013 21st International Conference on Geoinformatics, Kaifeng, China, 20–22 June 2013; pp. 1–5.
36. Zhang, X.; Wang, T.; Jiao, D.; Zhou, Z.; Yu, J.; Cheng, X. Detecting inconsistent information in crowd-sourced street networks based on parallel carriageways identification and the rule of symmetry. *ISPRS J. Photogramm. Remote Sens.* **2021**, *175*, 386–402. [[CrossRef](#)]
37. Chen, J.; Liu, W.; Li, Z.; Zhao, R.; Cheng, T. Detection of spatial conflicts between rivers and contours in digital map updating. *Int. J. Geogr. Inf. Sci.* **2007**, *21*, 1093–1114. [[CrossRef](#)]
38. Ai, T.; Yang, M.; Zhang, X.; Tian, J. Detection and correction of inconsistencies between river networks and contour data by spatial constraint knowledge. *Cartogr. Geogr. Inf. Sci.* **2015**, *42*, 79–93. [[CrossRef](#)]
39. Mazuran, M.; Tipaldi, G.D.; Spinello, L.; Burgard, W.; Stachniss, C. A statistical measure for map consistency in SLAM. In Proceedings of the 2014 IEEE International Conference on Robotics and Automation (ICRA), Hong Kong, China, 31 May–7 June 2014; pp. 3650–3655.
40. Iakovidou, C.; Zampoglou, M.; Papadopoulos, S.; Kompatsiaris, Y. Content-aware detection of JPEG grid inconsistencies for intuitive image forensics. *J. Vis. Commun. Image Represent.* **2018**, *54*, 155–170. [[CrossRef](#)]
41. Herold, M.; Mayaux, P.; Woodcock, C.E.; Baccini, A.; Schmullius, C. Some challenges in global land cover mapping: An assessment of agreement and accuracy in existing 1 km datasets. *Remote Sens. Environ.* **2008**, *112*, 2538–2556. [[CrossRef](#)]
42. Yu, L.; Zhang, D.; Holden, E.-J. A fast and fully automatic registration approach based on point features for multi-source remote-sensing images. *Comput. Geosci.* **2008**, *34*, 838–848. [[CrossRef](#)]
43. Zhao, C.; Goshtasby, A.A. Registration of multitemporal aerial optical images using line features. *ISPRS J. Photogramm. Remote Sens.* **2016**, *117*, 149–160. [[CrossRef](#)]
44. Hsieh, Y.C.; McKeown, D.M.; Perlant, F.P. Performance evaluation of scene registration and stereo matching for cartographic feature extraction. *IEEE Trans. Pattern Anal. Mach. Intell.* **1992**, *14*, 214–238. [[CrossRef](#)]
45. Livi, L.; Rizzi, A. The graph matching problem. *Pattern Anal. Appl.* **2013**, *16*, 253–283. [[CrossRef](#)]
46. Mena, J.B. State of the art on automatic road extraction for GIS update: A novel classification. *Pattern Recognit. Lett.* **2003**, *24*, 3037–3058. [[CrossRef](#)]
47. Fuchs, R.; Verburg, P.H.; Clevers, J.G.P.W.; Herold, M. The potential of old maps and encyclopaedias for reconstructing historic European land cover/use change. *Appl. Geogr.* **2015**, *59*, 43–55. [[CrossRef](#)]
48. Roussel, J.-R.; Bourdon, J.-F.; Morley, I.D.; Coops, N.C.; Achim, A. Correction, update, and enhancement of vectorial forestry road maps using ALS data, a pathfinder, and seven metrics. *Int. J. Appl. Earth Obs. Geoinf.* **2022**, *114*, 103020. [[CrossRef](#)]
49. Wang, S.; Quan, D.; Liang, X.; Ning, M.; Guo, Y.; Jiao, L. A deep learning framework for remote sensing image registration. *ISPRS J. Photogramm. Remote Sens.* **2018**, *145*, 148–164. [[CrossRef](#)]
50. Hoskins, A.J.; Bush, A.; Gilmore, J.; Harwood, T.; Hudson, L.N.; Ware, C.; Williams, K.J.; Ferrier, S. Downscaling land-use data to provide global 30" estimates of five land-use classes. *Ecol. Evol.* **2016**, *6*, 3040–3055. [[CrossRef](#)]
51. Yu, J.; Li, X.; Guan, X.; Shen, H. A remote sensing assessment index for urban ecological livability and its application. *Geo-Spat. Inf. Sci.* **2022**, 1–22. [[CrossRef](#)]
52. Ling, F.; Du, Y.; Xiao, F.; Xue, H.; Wu, S. Super-resolution land-cover mapping using multiple sub-pixel shifted remotely sensed images. *Int. J. Remote Sens.* **2010**, *31*, 5023–5040. [[CrossRef](#)]
53. Shen, Y.; Ai, T. A Raster-Based Methodology to Detect Cross-Scale Changes in Water Body Representations Caused by Map Generalization. *Sensors* **2020**, *20*, 3823. [[CrossRef](#)]

54. Shen, Y.; Ai, T.; Li, W.; Yang, M.; Feng, Y. A polygon aggregation method with global feature preservation using superpixel segmentation. *Comput. Environ. Urban Syst.* **2019**, *75*, 117–131. [[CrossRef](#)]
55. Tinghua, A.; Jingzhong, L. The lifespan model of GIS data representation over scale space. In Proceedings of the 2009 17th International Conference on Geoinformatics, Fairfax, VA, USA, 12–14 August 2009; pp. 1–6.
56. Venkatesan, R.; Koon, S.M.; Jakubowski, M.H.; Moulin, P. Robust image hashing. In Proceedings of the Proceedings 2000 International Conference on Image Processing (Cat. No.00CH37101), Vancouver, BC, Canada, 10–13 September 2000; Volume 3, pp. 664–666.
57. Shen, Y.; Ai, T. A Hierarchical Approach for Measuring the Consistency of Water Areas between Multiple Representations of Tile Maps with Different Scales. *ISPRS Int. J. Geo-Inf.* **2017**, *6*, 240. [[CrossRef](#)]
58. Lowe, D.G. Distinctive Image Features from Scale-Invariant Keypoints. *Int. J. Comput. Vis.* **2004**, *60*, 91–110. [[CrossRef](#)]
59. Achanta, R.; Shaji, A.; Smith, K.; Lucchi, A.; Fua, P.; Süsstrunk, S. SLIC Superpixels Compared to State-of-the-Art Superpixel Methods. *IEEE Trans. Pattern Anal. Mach. Intell.* **2012**, *34*, 2274–2282. [[CrossRef](#)] [[PubMed](#)]
60. Shen, Y.; Ai, T.; Wang, L.; Zhou, J. A new approach to simplifying polygonal and linear features using superpixel segmentation. *Int. J. Geogr. Inf. Sci.* **2018**, *32*, 2023–2054. [[CrossRef](#)]
61. Töpfer, F.; Pillewizer, W. The Principles of Selection. *Cartogr. J.* **1966**, *3*, 10–16. [[CrossRef](#)]

Disclaimer/Publisher’s Note: The statements, opinions and data contained in all publications are solely those of the individual author(s) and contributor(s) and not of MDPI and/or the editor(s). MDPI and/or the editor(s) disclaim responsibility for any injury to people or property resulting from any ideas, methods, instructions or products referred to in the content.